



Impact of hybridization on metallic-glass formation and design

C.C. Yuan^{1,2,3,*}, F. Yang², X.K. Xi⁴, C.L. Shi⁴, D. Holland-Moritz², M.Z. Li⁵, F. Hu¹, B.L. Shen^{1,*}, X.L. Wang³, A. Meyer², W.H. Wang⁴

¹ School of Materials Science and Engineering, Jiangsu Key Laboratory for Advanced Metallic Materials, Southeast University, Nanjing 211189, China

² Institut für Materialphysik im Weltraum, Deutsches Zentrum für Luft- und Raumfahrt (DLR), 51170 Köln, Germany

³ Department of Physics, City University of Hong Kong, 83 Tat Chee Avenue, Kowloon, Hong Kong, China

⁴ Institute of Physics, Chinese Academy of Sciences, Beijing 100190, China

⁵ Department of Physics, Beijing Key Laboratory of Opto-electronic Functional Materials and Micro-nano Devices, Renmin University of China, Beijing 100872, China

The formation mechanism of glass at the atomic scale has been under debate over centuries. In this work, we demonstrate that hybridization, as manifested by Mott's pseudogap, has a strong influence on the bond length as well as atomic packing, which can potentially tailor the formation of metallic glasses at microscopic time and length scales. A $p-d$ orbital hybridization between the post-transition metal Al and the transition metal was shown by the ^{27}Al isotropic shifts and the spin-lattice relaxation time of Zr-Co-Al alloys using nuclear magnetic resonance. These bonds lead to a charge transfer between the specific atomic pairs and the shrinkage of interatomic distances. Such chemical bonding favors the formation of metallic glasses by introducing a string-like structure and further stabilizes metallic glasses via a reduction in the density of states at the Fermi level. Our work has implications for understanding the glass formation mechanism at the electronic level and may open up new possibilities on the design of glass from the perspective of atomic interactions.

Introduction

Compared with rubbers, optical fibers, and numerous other glasses found in nature or produced for industrial applications, metallic glasses (MGs) are considered to exhibit more random atomic packing without directional bonding [1–3]. Generally, freezing of atomic dynamics in MGs during glass transition occurs via localization of atoms by their neighbors [4,5]. The densification of packing rather than bonding nature, thus, is proposed to play a dominant role during glass transition and in determining the MG's formation [3–10].

Nevertheless, unlike one component hard-sphere systems, the description of the real packing state of MGs is controversial. For

multi-component MGs that typically exhibit a strong chemical short-range order [11–14], the local packing density of the atoms may deviate from the calculated macroscopic average packing density. Moreover, the atomic size in alloys is not well defined. The atomic radius could differ from that of the pure element, and in some cases may even depend on the alloy composition. A significant shortening of the bonds between transition metal (TM)-Al atomic pairs has been found, e.g. in $\text{Zr}_{46}\text{Cu}_{47}\text{Al}_7$ [13] and $\text{Al}_{87}\text{Ni}_7\text{Nd}_6$ [14] MGs. Hence, the packing density cannot be used as a convincing parameter to describe glass formation, particularly when different alloy systems with dissimilar chemical environments are compared. For example, Zr-Ni displays a higher density of packing than Zr-Cu in the liquid state [15]. It is, however, a worse glass former compared to Zr-Cu.

Theoretical calculations show that a composition dependence of the density of packing originates from chemical/electronic

* Corresponding author at: School of Materials Science and Engineering, Jiangsu Key Laboratory for Advanced Metallic Materials, Southeast University, Nanjing 211189, China.

E-mail address: Yuan, C.C. (yuanchenchenne@hotmail.com)

interactions between the alloy components [11–13], which significantly affect atomic configurations [11–14] and macroscopic properties of MGs, e.g. Hall coefficient, conductivity, magnetoresistance, elastic modulus/stiffness, plasticity, and toughness [16–21]. It makes us wonder how such chemical effects influence the formation of MGs. Some studies suggest that the stability of MGs relies on Mott's pseudogap or chemical bonding/valence electron concentration under the framework of Nagel-Tauc's nearly-free-electron model [22–25]. However, the experimental verification of these correlations is still far from conclusive [26–28]. A detailed investigation of the extended partial density of states (DOS), such as *s*- and *p*-DOS, is lacking, especially for *sp* elements like P and Al with low photoionization cross-sections [27]. Besides, classical structural models [1,8,12,29,30] for describing MGs formation, such as Bernal's dense random packing model [1], focus more on atomic sizes and topological configurations. The details of the bonding nature are rarely taken into account [29,30].

The present work aims to figure out the role of the electronic state on atomic packing and its impact on glass formation. Nuclear magnetic resonance (NMR) measurements and *ab initio* molecular dynamics simulations are conducted here to trace the evolution of the local electronic configuration of ^{27}Al nuclei in typical TM-Al glass-forming Zr–Co–Al alloys. NMR spectroscopy is a powerful experimental tool for characterizing the electronic/band state of MGs in the vicinity of the Fermi level [31,32]. More importantly, ^{27}Al NMR has been proved as an atomic probe to describe the *s*-DOS in a TM matrix well [33–36]. Aluminum is of special interest from the MGs development point of view since it is known as an effective additive that is slowing down the atomic dynamics [37,38] and improving the glass-forming ability (GFA) [39]. Moreover, a tiny amount of Al can simultaneously enhance the yield strength and compressive plasticity of MGs considerably [40,41].

Combined with density measurements on highly reactive Zr–Co–Al melts by utilizing advanced containerless processing techniques [42], we found that changes of the GFA as a function of the Al concentration are not resulting from variations of the density of packing but are controlled by an increased amount of covalent-like bonding. Hybridization indicated by Mott's pseudogap in NMR studies leads to a minimum of the DOS at the Fermi level, which causes that the maximum stability of the material occurs upon saturation of the covalent-like bonds. On the other hand, hybridization results in a charge transfer between the specific atomic pairs and bond shortening. Such chemical/directional bonds facilitate the formation of energetically favorable molecular-like fragments, which leads to e.g. sluggish atomic dynamics [38] and/or the stabilization of liquid phases. Our studies based on NMR and *ab initio* simulations provide not only a characterization of the bonding nature in MGs but also a deep insight into the underlying physical mechanism of MG formation. It may further promote the design and manufacturing of function-improved MGs by considering of influences resulting from atomic interactions.

Results

Concentration dependence of the GFA and the average packing fraction in Zr–Co–Al alloys

The critical diameters D for glass formation as well as the width of the supercooled regime ($\Delta T_x = T_g - T_x$) of $\text{Zr}_{72-x}\text{Co}_{28}\text{Al}_x$

($4 \leq x \leq 24$) are plotted in Fig. 1a and b as characterizations of the GFA, where T_g and T_x are the glass transition temperature and crystallization onset temperature, respectively. The critical diameters for alloys containing 14 and 16 at.% Al are taken from the work of Wada [43] and Yu et al. [44], and the data for other compositions are measured in this work. It can be seen that the widest ΔT_x of 55 K was observed at $x = 16$ at.% Al, indicating a thermally most stable supercooled state at this composition. This agrees well with the largest critical diameter of 18 mm found for $\text{Zr}_{56}\text{Co}_{28}\text{Al}_{16}$ [43].

Density, molar volume, and packing fraction of Zr–Co–Al melts at 1300 K are presented in Fig. 1d–f as a function of the Al concentration. All measured densities show a linear dependence with the temperature down to the undercooled state, giving no indication for volume-change involved transitions, such as liquid–liquid phase transitions [45], within the investigated temperature and composition range. The typical density–temperature relations of $\text{Zr}_{72-x}\text{Co}_{28}\text{Al}_x$ ($4 \leq x \leq 24$) melts are shown in Fig. 1c. These melts exhibit a similar thermal expansion coefficient for all compositions. Consistent with the lower density of Al compared with that of both Zr and Co, the density ρ of Zr–Co–Al melts decreases with Al addition. The covalent/Goldschmidt radius (r^c , r^G) of Al ($r_{\text{Al}}^c = 1.248 \text{ \AA}$, $r_{\text{Al}}^G = 1.43 \text{ \AA}$) is between that of Zr ($r_{\text{Zr}}^c = 1.454 \text{ \AA}$, $r_{\text{Zr}}^G = 1.60 \text{ \AA}$) and Co ($r_{\text{Co}}^c = 1.157 \text{ \AA}$, $r_{\text{Co}}^G = 1.26 \text{ \AA}$) [46,47]. Therefore, the specific molar volume V_m ($V_m = \bar{M}/\rho$, where \bar{M} is the average molar mass of all components) decreases with increasing Al concentration in cases of both $\text{Zr}_{72-x}\text{Co}_{28}\text{Al}_x$ and $(\text{Zr}_{0.67}\text{Co}_{0.33})_{100-x}\text{Al}_x$, where (mainly) large Zr is substituted by Al, whereas it increases in the case of $\text{Zr}_{56}\text{Co}_{44-x}\text{Al}_x$, where small Co is substituted by Al.

The average packing fraction ϕ that describes the packing state of a system independent of atomic size and mass is plotted in Fig. 1f. ϕ is derived by assuming hard-sphere-like packing using $\phi = N_A \hat{V}/V_m$ (Ref. [38]), where N_A is Avogadro's number and \hat{V} the effective size of the atoms calculated by $\hat{V} = 4/3\pi(r^3)$ using the fixed covalent/Goldschmidt radii (r) of the pure metals [46,47]. When considering the experimental error limits of $\pm 5\%$, no significant variation of the packing fraction ϕ is observed. This clearly manifests that changes of the average packing density are not responsible for the observed dependence of the GFA on the Al concentration. Considering the changes of the atomic packing during the crystallization of alloys [6,7], a comparison of ϕ is also made between that of the crystalline $\text{Zr}_{72-x}\text{Co}_{28}\text{Al}_x$ alloys and their melts of the same composition. The difference in the ϕ between the melt at 1300 K and the crystallized material at ambient temperature is about 3%, which changes very weakly with composition.

NMR investigations on Zr–Co–Al glass

Different from the behavior of ϕ , the local band state at Al sites shows a clear correlation with the GFA. The isotropic Knight shifts (K_{iso}) and the spin–lattice relaxation times (T_1) observed in NMR spectra (Fig. 2) display a maximum and minimum, respectively, for the best glass former. K_{iso} of Al has been correlated with the electronic structure and the bonding character in MGs. The orbital contribution for an *sp* element like Al, which only has *s* and *p* electronic orbitals, is usually small [33–35].

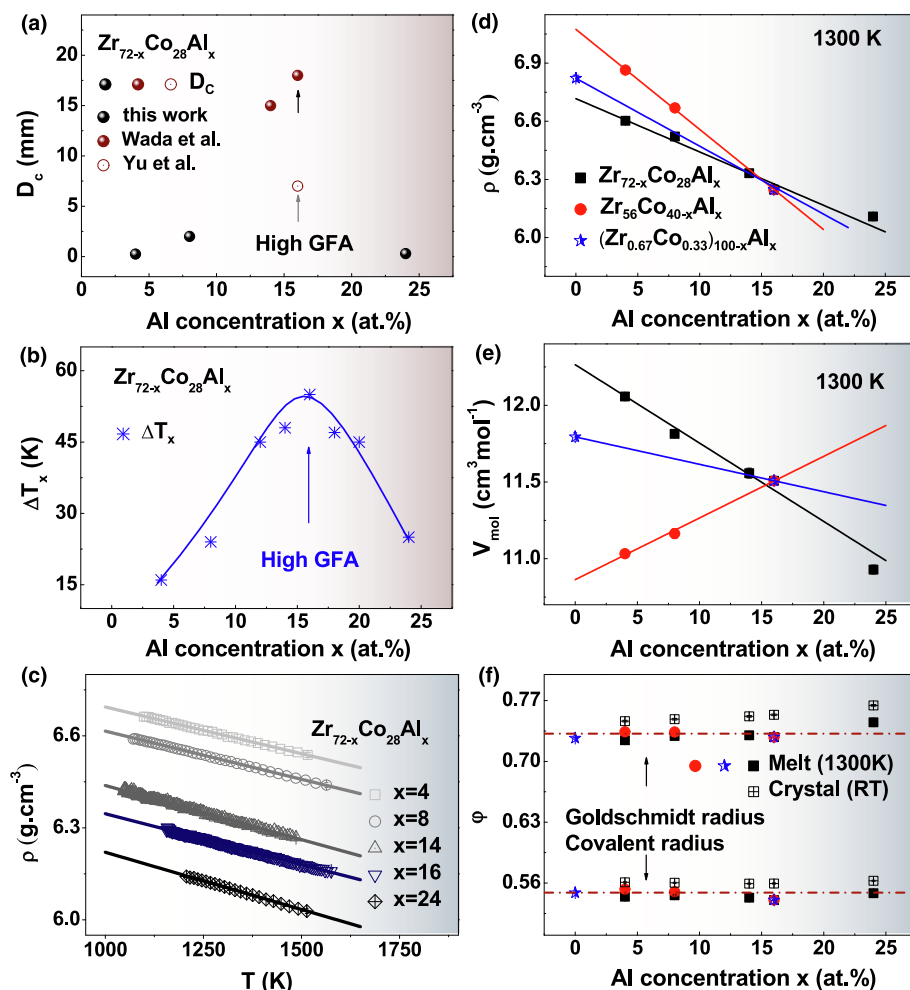


FIGURE 1

GFA, density, molar volume, and packing fraction of Zr–Co–Al. (a) Critical diameter for glass-formation D_c and (b) supercooled regime ΔT_x of $\text{Zr}_{72-x}\text{Co}_{28}\text{Al}_x$ with $4 \leq x \leq 24$. The critical diameters for the compositions with 14 and 16 at.% Al addition are from the work of Wada [43] and Yu et al. [44]. (c) Density ρ as a function of the temperature for molten $\text{Zr}_{72-x}\text{Co}_{28}\text{Al}_x$ ($x = 4, 8, 14, 16, 24$). (d) Density ρ , (e) molar volume V_{mol} , and (f) effective volume packing fraction ϕ of $\text{Zr}_{72-x}\text{Co}_{28}\text{Al}_x$, $\text{Zr}_{56}\text{Co}_{40-x}\text{Al}_x$, and $(\text{Zr}_{0.67}\text{Co}_{0.33})_{28}\text{Al}_x$ melts ($4 \leq x \leq 24$) at 1300 K. The solid in (b) and the dash lines in (f) are guides for eyes. The solid lines in (c), (d), and (e) are the linear fits to the experimental data.

Hereby, ^{27}Al NMR isotropic shifts can be simplified as $K_{\text{iso}} = \frac{16\pi}{3} \mu_B^2 \langle |\psi(0)|^2 \rangle_{E_F} g_s(E_F)$, where μ_B is the Bohr magneton, $\langle |\psi(0)|^2 \rangle_{E_F}$ the average probability density at the nucleus for electronic states on the Fermi surface, and $g_s(E_F)$ the DOS of s electrons at the Fermi level (E_F). A notable reduction in the ^{27}Al K_{iso} with a small amount of Al addition ($x < 8$) in $\text{Zr}_{72-x}\text{Co}_{28}\text{Al}_x$ (466–477 ppm) (see region a in Fig. 2) as compared with that of pure metallic Al (~ 1630 ppm) [21,35] shows that the $g_s(E_F)$ at Al sites in Zr–Co–Al MGs is significantly reduced compared to pure Al. This indicates that E_F is located near a pseudogap-like minimum of the Al s sub-band, suggesting a pronounced p – d orbital hybridization of TM and Al [16,17]. Similar observations have been reported in several TM–Al compounds [21,33–35].

From the previous investigation of Co–Al [17], or Zr–late TM (Cu, Ni, Co)–Al MGs [21], E_F is also located at the Co $3d$ and Zr $4d$ hybridized bonding region. Due to the much higher d -DOS at E_F of Co compared to that of Zr [19], the exchange core polarization effect of the Co $3d$ orbital on K_{iso} is dominant [21]. There-

fore, similar to the studies of other weakly paramagnetic TM–metalloid-based MGs [33,34], the observed ^{27}Al NMR shifts in Zr–Co–Al MGs are also contributed from the $g_d(E_F)$ at the Co sites via exchange core polarization. The slight shift of K_{iso} to a higher position for $\text{Zr}_{56}\text{Co}_{28}\text{Al}_{16}$ (see region b in Fig. 2) suggests a higher overlap among Al $3p$ and Co $3d$ states in the energy space [21], which indicates a high degree of the occupation of Co–Al hybridized bonding states, i.e. covalent-like/directional bonding.

With further addition of Al from 16 to 24 at.%, the ^{27}Al K_{iso} decreases from 483 to 457 ppm at a magnetic field of 9.39 T, as shown in Fig. 2 (region c). This phenomenon suggests the saturation of covalent-like bonding of Al at the composition with 16 at.% Al addition. It is similar to the case of the reduction in ^{59}Co K_{iso} upon the super-saturation of B in the Co–B solid solution at a composition of $\text{Co}_{73}\text{B}_{27}$ [32].

We also find that T_1 is only about 19.8 ms in the $\text{Zr}_{56}\text{Co}_{28}\text{Al}_{16}$ glass, which is much shorter than the values for Zr–Cu–Al [35] or Zr–Cu–Ni–Al–Sn [20] MGs of approximately 100 ms. In these Zr-based MGs [20,35], the ^{27}Al T_1 is related to the Korringa relax-

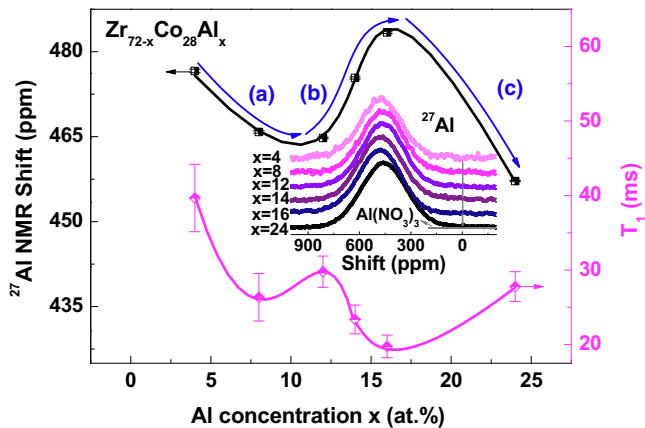


FIGURE 2

NMR studies on amorphous $Zr_{72-x}Co_{28}Al_x$ ribbons with $4 \leq x \leq 24$. Knight shift (left axis) and spin–lattice relaxation time T_1 (right axis) as a function of the Al concentration. The inset shows ^{27}Al NMR central line shapes of powder spectra of $Zr_{72-x}Co_{28}Al_x$ MGs; an ^{27}Al NMR spectrum of $Al(NO_3)_3$ is shown as a reference of zero shift. All ^{27}Al NMR spectra are normalized to the maximum intensity and taken at $H = 9.39$ Tesla and $T = 298$ K. The solid lines in the inset are fitted with a Gaussian distribution.

ation that originates from the hyperfine interactions between the conduction electrons and nuclear spins. Therefore, the fast spin–lattice relaxation process for the best glass former suggests that the GFA of Zr–Co–Al MGs is closely bound up with the orbital hybridization effects.

Ab initio molecular dynamics analysis

The *ab initio* calculated DOS of $Zr_{56}Co_{28}Al_{16}$ MGs further confirms the results of NMR studies, exhibiting a significantly hybridized band indicated by the overlap of the peaked Co 3d and Zr 4d resonances with the Al 3p band at $-4 \text{ eV} < E - E_F < 1.35 \text{ eV}$, as shown in Fig. 3a. More interestingly, we find a low lying plateau in the broadened TM *d* sub-bands close to E_F accompanied by the localized *s* electrons around Al sites (a narrow 3s-Al band with the energy interval from -7.5 to -5 eV , with a maximum at -5.4 eV), corresponding to a Mott's pseudogap as predicted by Nagel et al. [22]. Our studies show that the hybridization causes that E_F lies at the pseudogap-like plateau of the total DOS, which has been proposed to stabilize MGs [22].

Fig. 3b displays the average Bader net charge of each element that represents the degree of covalent/ionized bonding [48]. As shown in the inset of Fig. 3b, the Bader net charge of Co and Zr fluctuates in the range from 1.4 to 1.6 and from -0.6 to -0.8 e , respectively, indicating that a substantial amount of electrons are transferred from Zr to Co. Such charge transfer as a result of the orbital hybridization is in line with the relative electronegativity of these components, namely, the tendency of an atom to attract electrons, which is 1.33, 1.88, and 1.61 for Zr, Co, and Al, respectively [49]. With increasing Al concentration, the Bader net charge of Co slightly increases accompanied by a loss of charge for Zr, demonstrating an enhanced charge-transfer process, while the role of the Al atoms changes from the electron acceptors to the electrons donors. The Co–Al bonding (Al donates electrons to Co) instead of the Zr–Al bonding

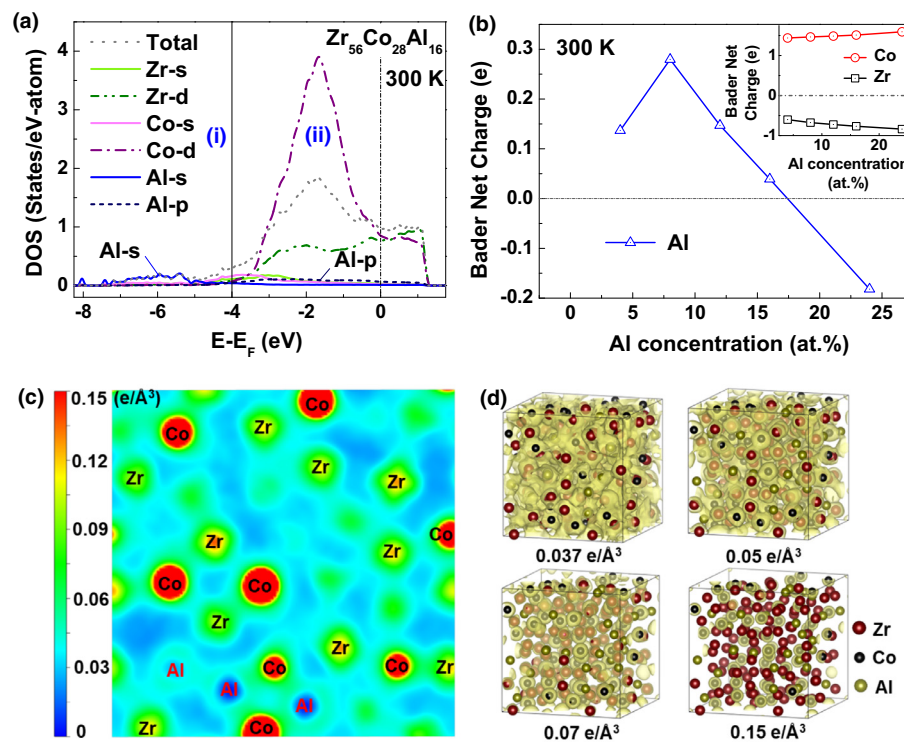


FIGURE 3

Ab initio molecular dynamics studies on the electronic structure of $Zr_{72-x}Co_{28}Al_x$ ($4 \leq x \leq 24$) at 300 K. (a) Projected total and partial DOS for $Zr_{56}Co_{28}Al_{16}$. (b) The Bader net charge as a function of the Al concentration. (c) Two-dimensional electron-density distribution in $Zr_{56}Co_{28}Al_{16}$. (d) Isosurface of the charge density of the band B with isosurface levels of 0.037, 0.05, 0.07, and $0.15 \text{ e}/\text{\AA}^3$.

(Al accepts electrons from Zr) becomes more pronounced upon Al addition (Fig. 3b). When the concentration of Al reaches 16 at.%, the Bader net charge of Al is close to 0. This suggests that the competition of the Co–Al and the Zr–Al bonding reaches a balance at the composition of the best GFA.

According to the peak position of the 3*d*-DOS of Co in the hybridized band, the partial DOS shown in Fig. 3a can be divided into i ($-8.2 \text{ eV} < E - E_F < -4 \text{ eV}$) and ii ($-4 \text{ eV} < E - E_F < 1.35 \text{ eV}$) bands. The selected slice of the electron-density distribution of the hybridized ii bands is drawn in Fig. 3c. One can clearly see that the charge density around Al atoms is significantly depressed as a result of the reduction in the 3*s*-DOS of Al at the E_F due to the *p*-*d* orbital hybridization of Al with TMs. The tunnel-like structure between Al and Co/Zr in the three-dimensional isosurface shown in Fig. 3d with a low charge-density level of about $0.037 \text{ e}/\text{\AA}^3$ further verifies the corresponding charge redistribution and the covalent-like bonding. An observable electronic transfer from Zr to Co is also indicated by the tubes appearing between the charge isosurface of Co and Zr within a charge density range from 0.05 to $0.07 \text{ e}/\text{\AA}^3$, as well as the high electron-density around the Co atoms shown in the isosurface with a high-level charge density of $0.15 \text{ e}/\text{\AA}^3$.

In order to provide a vivid image of the chemical interaction between the alloy components, the typical atomic configurations of Co and Al atoms bonded within the first-coordination shell are drawn in Fig. 4a for a melt at $T = 1300 \text{ K}$. It can be seen that a connective structure is formed due to directional bonds between Co–Al atomic pairs. String-like atomic configurations are observed in Fig. 4a. When $x \leq 16$, short chains are dominant. As seen in

Fig. 4b, only Co–Al strings with the atomic number (AN) of 2 are found for the composition with 4 at.% Al. The number of strings with AN = 2 at $x = 4$ is 6. It reaches a maximum value of 10 at $x = 12$ and then decreases. With increasing Al concentration, the AN of the longest strings and the total number of strings (AN = 2–6) in each system rise simultaneously, as shown in Fig. 4b and c. The maximum length of the strings and the number of long fragments with AN = 4, 6 reach a maximum value at $x = 16$.

The partial coordination numbers z_{ij} derived by integrating the radial distribution functions up to the first minimum are listed in Table 1. The large coordination number z_{iZr} that represents the number of Zr atoms surrounding an atom of type *i* ($i = \text{Co, Al}$) demonstrates that both Al and Co prefer to be surrounded by Zr as the nearest neighbors, avoiding nearest neighbors of the same type. A similar lack of direct Al–Al contacts (solute–solute avoidance) has also been observed in Zr–Cu–Al [36]. The formation of Co–Al chains, thus, facilitates the construction of a connective configuration via interlinking the short-range Zr–Co and Zr–Al pairs, which may retard the crystallization of Zr–Co–Al melts. Furthermore, the string-like clusters/motion-paths impede atomic motion during glass transition via cooperatively rearranging particles [50,51]. With further increase in the Al concentration, short chains become dominant again. For instance, at $x = 24$ the maximum of the distribution of AN is found at AN = 3 with a maximum value of 10. As shown before, also the GFA decreases for Al concentrations above 16 at.%. This manifests that the dependence of the GFA on the Al concentration may result from the formation of the chain-

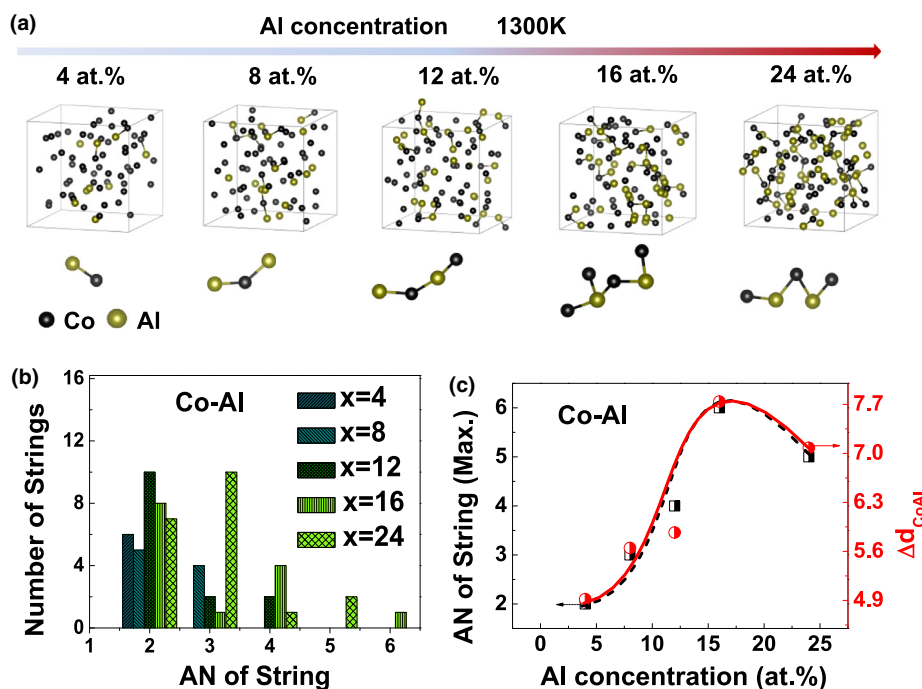


FIGURE 4

Atomic configurations of $\text{Zr}_{72-x}\text{Co}_{28}\text{Al}_x$ ($4 \leq x \leq 24$) at 1300 K. The dark and yellow balls in (a) represent Co and Al atoms, respectively. (a) Configurations of bonded Co–Al atomic pairs. (b) Number of strings as a function of the number of atoms (AN) in the string. (c) Maximum AN of the strings (AN of String (Max.)), i.e. the AN of the longest string as a function of the Al concentration (left axis) and the shortening of the Co–Al bonds Δd_{CoAl} (right axis) as a function of the Al concentration.

TABLE 1

Number of nearest-neighbors z_{ij} and coordination numbers z_i for different pairs of atoms in ternary $Zr_{72-x}Co_{28}Al_x$ ($4 \leq x \leq 24$) melts at 1300 K.												
Z_{ij} Z_i	Z_{ZrZr}	Z_{ZrCo}	Z_{ZrAl}	Z_{CoZr}	Z_{CoCo}	Z_{CoAl}	Z_{AlZr}	Z_{AlCo}	Z_{AlAl}	Z_{Zr}	Z_{Co}	Z_{Al}
$Zr_{68}Co_{28}Al_4$	9.55	3.59	0.53	8.72	1.89	0.41	9.03	2.85	0.31	13.67	11.02	12.18
$Zr_{64}Co_{28}Al_8$	9.06	3.67	1.11	8.39	1.87	0.84	8.85	2.93	0.57	13.84	11.09	12.35
$Zr_{60}Co_{28}Al_{12}$	8.40	3.71	1.71	7.96	1.80	1.19	8.53	2.77	0.91	13.82	10.94	12.21
$Zr_{58}Co_{28}Al_{14}$	8.21	3.79	2.08	7.85	2.02	1.35	8.61	2.70	1.07	14.08	11.23	12.37
$Zr_{56}Co_{28}Al_{16}$	7.93	3.78	2.42	7.56	1.91	1.72	8.47	3.01	1.04	14.13	11.19	12.53
$Zr_{48}Co_{28}Al_{24}$	6.90	3.95	3.73	6.77	1.93	2.84	7.47	3.31	2.08	14.58	11.53	12.86

like structure with hybridized bonding that is most pronounced at the composition of the best GFA.

Discussion

Chemical bonding as a result of hybridization is associated with a significantly shortened distance of Co–Al atomic pairs, as shown in Fig. 4c. The shortening of the bonds is expressed as $\Delta d_{ij}(\%) = \{(d_{ii} + d_{jj})/2 - d_{ij}\} / \{(d_{ii} + d_{jj})/2\}$. d_{ij} s are the nearest-neighbor distances of all i – j atomic pairs, which are determined from the first peaks of the partial pair-correlation functions $g_{ij}(r)$. The data are listed in Table 2. For the best glass former, $Zr_{56}Co_{28}Al_{16}$, Δd s amount to 10.18%, 7.74%, and 0.74% for Zr–Co, Co–Al, and Zr–Al atomic pairs at 1300 K, respectively. Δd_{ZrCo} , Δd_{CoAl} , and Δd_{ZrAl} almost increase monotonously with Al addition. It is found that similar to other Al-containing melts [13,14], here at least part of the interatomic distances are composition dependent, i.e., depending on the degree of covalent bonding nature. Therefore, the calculation of packing fractions (see in Fig. 1f) that is based on a simple hard-sphere picture using constant atomic radii [9] is actually unrealistic. Our results highlight that the real MGs are not well described by such a simple hard-sphere approach and that the characteristics of the atomic interactions are of fundamental importance for understanding the mechanisms of glass formation.

In fact, a covalent-like bond character has a large impact on the topological arrangements of atoms in liquids/MGs [30,52]. In a simple metal system, e.g., the monoatomic melt of a pure transition metal [53], the population of icosahedra/icosahedra-like configurations with five-fold symmetry is pronounced. However, for metalloid-metal-based systems, such as Fe–(Si, P, C, B) [12,30] and $Pd_xNi_{80-x}P_{20}$ [52], covalent bonds result in the formation of prism-type motifs. Here, we show that for Zr–Co–Al melts string-like configurations play an important role, where the energetically favorable Co–Al bonds are formed. Such chain-like motifs can be found in both glassy and liquid state, which might be the reason for sluggish atomic dynamics of this system [38].

The improvement of the GFA by minor element addition is often discussed in terms of an enhancement of the packing efficiency or atomic size mismatch [9,10,54]. Nevertheless, the atomic-level packing efficiency may be affected by the degree of hybridization due to the composition-dependent shortening of bonds, particularly for those MGs containing metalloid-like elements, e.g., Zr–Cu–Al [13,29], Al–Ni–Nd [14], and the present studied Zr–Co–Al. Besides, the change of atomic packing introduced upon alloying a small portion of atoms is not so remarkable if only the atomic size difference is considered. In contrast, the local electronic/band state and the correlated atomic configurations are more sensitive to the small change of alloy compositions [13,52,55]. Moreover, other properties related to the GFA, such as melt dynamics, are prone to be influenced by bonding nature [37,38]. Therefore, hybridization is likely the origin of microalloying effects.

The correlation between the electronic state and the glass formation in MGs has already drawn attention since 1975 [22], even though convincing experimental proofs are rare [26,28]. With the advances in the computer simulation, its manifestations have been revealed in more and more details for an increasing number of MGs. Particularly, the occurrence of bond shortening [13,14] and the specific structural motifs [12,30,52] in glass-forming alloy systems are shown to have clear electronic origins. For example, the shrinkage of the bond length between Cu–Al atomic pairs due to the coupling between the broad conduction band of Al and the narrow low-lying d band of late transition metals has been found in $Zr_{46}Cu_{47}Al_7$ MG [13]. Some simulations suggest that Mott's pseudogap may have a direct correlation with the GFA of MGs. For instances, in typical transition-metal-Al-based $Al_{86}Ni_{14-x}La_x$ ($x = 3, 5, 9$) MGs, *ab initio* calculations show a local minimum of the electronic DOS nearby E_F at the best glass-forming composition [25]. A similar pseudogap in the profile of TM- d has also been observed in the simulations of transition-metal-non-metal-based MGs, such as Pd–Ni–P [52], Fe–B [56], and Fe–P–C [57]. Moreover, similar to the saturation of covalent bonds found at the best glass-forming

TABLE 2

d_{ij} and Δd_{ij} (%) for different ij pairs of atoms in ternary $Zr_{72-x}Co_{28}Al_x$ ($4 \leq x \leq 24$) melts at 1300 K.

d_{ij} (Å)	d_{ZrZr}	d_{ZrCo}	d_{ZrAl}	d_{CoCo}	d_{CoAl}	d_{AlAl}	Δd_{ZrCo}	Δd_{ZrAl}	Δd_{CoAl}
$Zr_{68}Co_{28}Al_4$	3.16	2.58	2.91	2.55	2.47	2.64	9.54	−0.50	4.92
$Zr_{64}Co_{28}Al_8$	3.15	2.59	2.92	2.56	2.47	2.67	9.51	−0.30	5.65
$Zr_{60}Co_{28}Al_{12}$	3.19	2.58	2.94	2.57	2.48	2.70	10.33	0.27	5.87
$Zr_{58}Co_{28}Al_{14}$	3.18	2.58	2.92	2.56	2.45	2.71	10.15	0.91	7.01
$Zr_{56}Co_{28}Al_{16}$	3.18	2.58	2.93	2.57	2.44	2.72	10.18	0.74	7.74
$Zr_{48}Co_{28}Al_{24}$	3.18	2.59	2.91	2.57	2.45	2.70	10.12	1.11	7.08

composition of Zr–Co–Al, a covalence-dominated bonding behavior occurs in Pd₄₀Ni₄₀P₂₀ (one of the best-known glass formers up to now [58]) as demonstrated by the maximum value for the electron localization function between Ni and P [52]. These phenomena are consistent with our observations from NMR experiments, implying a significant impact of hybridization on the formation of MGs.

As proposed in the work of Mayou et al. [17], the strong hybridization is the underlying reason that causes E_F to lie at a pseudogap at the top of the d band, which leads to the maximum stability and/or the lowest electron energy of systems under the nearly-free-electron framework [22–25]. In other words, the best GFA or the most stable state of the supercooled liquid/glass can be achieved at the composition with the highest degree of hybridization or upon saturation of covalent bonds. Moreover, just like in the case of Zr–Co–Al, hybridization also results in the chemical/directional bonding. It may promote the formation of the energetically favorable chain-like motifs, which leads to the slowing down of liquid dynamics, particularly on approaching the glass transition [50]. This may also prevent the crystallization of the melt via the sluggish crystal-growth kinetics based on the diffusion-controlled mechanism at the deep undercooling [59]. In that way, the degree of hybridization, as characterized by, e.g. charge transfer, electronic localization [52], bond shortening [13], magnetic susceptibility [21,28], and NMR K_{iso} or T_1 [20,21,35], can be an important parameter for determining the formation of MGs.

Different empirical rules for predicting the GFA of MGs were established over the past decades [4,54,60–62]. Numerous GFA criteria have been proposed in terms of parameters based on their thermodynamic or kinetical properties (T_g , T_x , the liquidus temperature (T_l), the mixing enthalpy/entropy (ΔH^{mix} , ΔS^{mix}), the configurational entropy (ΔS_{config}), viscosity (η), etc.), such as $T_{rg} = T_g/T_l$, $\gamma = T_x/(T_g + T_l)$, $\gamma_m = (2T_x - T_g)/T_l$, $\gamma_c = (3T_x - 2T_g)/T_l$, $\delta = T_x/(T_l - T_g)$, $\varphi = T_{rg}(\Delta T_x/T_g)^{0.143}$, $\beta = T_x T_g/(T_l - T_x)^2$, $\beta' = T_x/(T_g + T_g/T_l)$, $\alpha = T_x/T_l$, $\zeta = T_g/T_l + \Delta T_x/T_x$, $\omega = T_g/T_x - 2T_g/(T_g + T_l)$, $\omega_2 = T_g/(2T_x - T_g) - T_g/T_l$, $\varepsilon = -\Delta S^{mix}/\Delta H^{mix}$, and the fragility of relaxing liquids (m or D) [4,54,60–62]. For the alloy series studied here, a correlation between the GFA and commonly used criteria like T_{rg} [63] or γ [64] is not so obvious [43,44] (see Supplemental Table S1). Nevertheless, the composition dependence of the GFA agrees well with the parameter ΔT_x and the degree of hybridization. The alloy with the best GFA (with 16 at.% Al addition) exhibits the widest ΔT_x and saturation of covalent bonds. This can be consistently understood by the fact that hybridization stabilizes the undercooled liquid or the glass against crystallization via affecting both the stability [22] and the mass transport [38] on atomic and/or microscopic time and length scale. Although such impact cannot be quantified here, combining the different aspects of glass formation, including packing and bonding hybridization, will allow for a better understanding of the underlying mechanisms of glass formation on a microscopic level.

In many alloy systems, the hybridization effect may be important and should be taken into account. For instance, for most of the currently reported bulk MG systems those contain nonmetals, metalloids/metalloid-like elements or post-transition metals (P, C, B, Al, Sn, Si, Ga, etc.) [54,60–62], the hybridization effect may have a decisive influence [13,22–27,35,52]. Moreover,

even in these systems where the hybridization/chemical effect is of lesser significance, such as the alloy systems consisting solely of early and/or late TMs with similar chemical properties, the evolution of bonding states as indicated by the degree of hybridization also needs to be considered [22,28]. For example, in a simple binary MG system like Zr–Cu, the change in magnetic susceptibility upon crystallization has been reported that closely relates to its GFA [28], although other atomic-scale properties or mechanisms, such as the local packing efficiency, may have an important contribution on the GFA of this system as well [6,7]. Nevertheless, due to the reason that the pseudogap hypothesis for describing the degree of hybridization starts from a nearly-free-electron model [17,22], the hybridization effect, in theory, isn't able to be used in those systems with extremely localized bonding states like wide-gap oxide glasses [65] or in hard-sphere systems without consideration of electronic interactions like the uncharged colloid system [66].

Bonding direction and flexibility are also known to play a key role in determining the mechanical properties of crystalline and amorphous alloys [19–21,67–70]. Owing to the hybridized bonding nature, even a small amount of additional elements has a large impact [20,69,70]. It induces the ductile-to-brittle transition in MGs via the shift of s -DOS far away from E_F , which leads to a catastrophic brittle fracture of the material for lack of the bond flexibility/mobility [20,70]. On the other hand, the strongly bonded clusters promote the generation of free volume between clusters [29] and cause hardening of the alloys [69], which improves both plasticity and toughness of the MGs. Here, we propose that such nanoscale structural heterogeneity together with high free volume [29,71] induced by the hybridized bonds of Al and TMs [20,21] might be the underlying mechanism for the enhanced plasticity/ductility (Poisson ratio) of Al-containing MGs [19,20,40,41].

As demonstrated here for the example of the Zr–Co–Al alloys, an analysis of the bonding characteristics provides a novel approach to design MGs with excellent performance. Similar to the role of Si–O covalent bonds in oxide glasses like the glassy silicate, the hybridized bonds between dissimilar metal elements or metals and nonmetals/metalloids, e.g. Co–Al [17], Pd–P [27], and Ca–Al [33] bonds, are the physical origin of strong atomic interactions. It stabilizes the MGs by inducing a pseudogap-like minimum of the DOS lies around E_F on account of the orbital hybridization [17]. Furthermore, the formation of loosely packed configurations based on a bonded network structure can solve the conflicts between the high GFA and the large plasticity in a number of MGs. In the framework of a simple hard-sphere model, a dense-packing state favors a high GFA [1,3–9], while a large plasticity demands more free volume (less dense packing) [29,71]. Besides, some other physical properties, such as conductivity and Hall coefficient of disordered systems, are also likely to be affected by the hybridization state [16,17]. The functionalities of potential amorphous semiconductors can be modulated by controlling the degree of hybridization through doping non-metallic/metalloid elements into amorphous metals [72].

In conclusion, a strong p – d hybridization between metalloid-like Al p and Co d orbitals in the Zr–Co–Al system is observed by NMR experiments. Such bonding leads to a redistribution of the Bader charge and to shortened interatomic distances as

shown in *ab initio* simulations. It stabilizes MGs by a decrease in the DOS at E_F and fosters the formation of string-like aggregates. This structural heterogeneity in the form of the directional bonding and atomic-scale chains might also contribute to the large plasticity of Al-containing MGs. Our studies highlight that the bonding characteristics can be used as a key parameter to evaluate and even to modulate the properties of less-ordered systems, such as MGs. This might help us to better understand the atomistic or electronic origin of glass transition and deformation mechanisms in glass-forming alloys.

Material and methods

Sample preparation

$Zr_{72-x}Co_{28}Al_x$ ($x = 4, 8, 14, 16, 24$ at.%) and $Zr_{56}Co_{44-x}Al_x$ ($x = 4, 8$ at.%) alloys for density measurement were prepared by arc melting of Zr (99.97 at.%, smart-elements), Co (99.998 at.%, Alfa Aesar), and Al (99.9999 at.%, Hydro Aluminum) in a Ti-gettered high-purity argon atmosphere (99.9999 at.%). Ribbons for NMR measurements with the thickness of ~ 30 μm were produced via the single roller melt spinning method. The amorphous nature of the ribbons was identified using X-ray diffraction with $Cu-K\alpha$ radiation.

Measurement of thermodynamic parameters

The parameters, such as T_g and T_x , were measured on amorphous ribbons and alloy ingots using differential scanning calorimetry (DSC, NETZSCH 404 F3) under a flow of high-purity argon (99.999 at.%) with a heating rate of 20 K/min.

Density measurements

The densities ρ of the highly reactive Zr–Co–Al melts were measured utilizing electrostatic levitation combined with a high-speed video diagnostic technique [42,45] over a wide temperature interval from 1025 to 1520 K. The projected area of the back-lighted sample was derived according to the average edge curve $\langle R(\varphi) \rangle = \sum_{i=1}^6 a_i P_i(\cos(\varphi))$, where $\sum_{i=1}^6 a_i P_i(\cos(\varphi))$ is a sum of Legendre polynomials up to the 6th order obtained by fitting the edge of the sample shadow, P_i the i th Legendre polynomial, a_i the prefactor for the i th Legendre polynomial, and φ the polar angle. Then, the sample volume V is calculated by using $V = \frac{2}{3}\pi \int \langle R(\varphi) \rangle^3 \sin\varphi d\varphi$, assuming rotation symmetry around the droplet normal to the projection direction. The density is then calculated from the volume and the mass of the sample. The temperature of the levitated sample was measured contactlessly using a single-color pyrometer that has been calibrated at the liquidus temperature T_l (as determined by DSC during melting), assuming a temperature independent emissivity. The uncertainty of the temperature measurement is of about ± 10 K [15]. A maximum undercooling of 225 K was achieved during the density measurements on the Zr–Co–Al system. The density of crystallized Zr–Co–Al alloys at ambient temperature was measured by the Archimedean method with an accuracy of $\pm 0.1\%$.

NMR measurements on K_{iso} and T_1

The ^{27}Al NMR measurements on amorphous ribbons of $Zr_{72-x}Co_{28}Al_x$ ($4 \leq x \leq 24$) were conducted at a magnetic field of 9.39 T. The ^{27}Al NMR free induction decay signal was recorded

using a two-pulse Hahn echo sequence, $90^\circ - \tau - 180^\circ$. The first pulse duration was kept as short as 6 μs to avoid a distortion of the central line transition. The signal was averaged within a recycle delay of 200 ms. The ^{27}Al K_{iso} is determined by the position of the intensity maxima or centroids of the Gauss-like central lines for the MGs [20] (the inset in Fig. 2). The T_1 was measured using the saturation recovery method with the same selective excitation as that of the spectra of ^{27}Al [31].

Ab initio molecular dynamics simulations

Ab initio molecular dynamics simulations of the $Zr_{72-x}Co_{28}Al_x$ ($4 \leq x \leq 24$) system were implemented in the Vienna *ab initio* simulation package using the projector augmented-wave method within the density-functional theory [73]. Canonical NVT (constant number, volume, temperature) ensembles containing 200 atoms in a cubic box with periodic boundary conditions were used. The initial atomic positions were generated randomly to maximize the Zr, Co, and Al mixing. The temperature was controlled with a Nose–Hoover thermostat. The liquid was equilibrated at 1725 K for 2000 time steps (3 fs per step) and then cooled down to 1300 and 300 K at a constant cooling rate of 0.24 K per step. The atomic configuration of the liquid at 1300 and 300 K was further relaxed isothermally for 5,000 time steps in order to analyze their structural properties statistically. The electronic structure and the charge transfer were determined using self-consistent charge densities with a $3 \times 3 \times 3$ k-point mesh for improving accuracy.

Acknowledgments

We thank Haiyang Bai, Baoan Sun, and Haibing Yu for stimulating discussions and Huaping Zhang for help in the ab-MD simulation. This work was supported by the National Natural Science Foundation of China (Grant Nos. 51601038 and 51631003), the Natural Science Foundation of Jiangsu Province, China (Grant No. BK20171354), Postdoctoral Fellow under the Hong Kong Scholar Scheme, China and Hong Kong (Grant No. XJ2017048), Jiangsu Key Laboratory for Advanced Metallic Materials (Grant No. BM2007204). XLW acknowledges the support by a grant from the Research Grants Council of the Hong Kong Special Administrative Region, Hong Kong (CityU 11216215) and the Croucher Foundation through the CAS-Croucher Foundation Joint Laboratory on Neutron Scattering (CityU 9500034).

Author contributions

C.C.Y. and F.Y. planned and carried out the experimental work. C.C.Y., C.L.S., X.K.X., and M.Z.L. analyzed the data. F.H. helped in preparing the samples for DSC and NMR measurements. C.C.Y., F.Y., D.H.M., and W.H.W. wrote the paper with input and advice from A.M., X.L.W., and B.L.S.

Appendix A. Supplementary data

Supplementary data to this article can be found online at <https://doi.org/10.1016/j.mattod.2019.06.001>.

References

- [1] J.D. Bernal, J. Mason, *Nature* 188 (1960) 910–911, <https://doi.org/10.1038/188910a0>.

- [2] A.L. Greer, *Science* 267 (1995) 1947–1953, <https://doi.org/10.1126/science.267.5206.1947>.
- [3] J. Schroers, *Phys. Today* 66 (2013) 32–37, <https://doi.org/10.1063/PT.3.1885>.
- [4] C.A. Angell, *Science* 267 (1995) 1924–1935, <https://doi.org/10.1126/science.267.5206.1924>.
- [5] A. Meyer, *Phys. Rev. B* 66 (13) (2002), <https://doi.org/10.1103/PhysRevB.66.134205> 134205.
- [6] Y. Li et al., *Science* 322 (2008) 1816–1819, <https://doi.org/10.1126/science.1163062>.
- [7] L. Yang et al., *Phys. Rev. Lett.* 109 (2012), <https://doi.org/10.1103/PhysRevLett.109.105502> 105502.
- [8] D. Turnbull, M.H. Cohen, *J. Chem. Phys.* 34 (1961) 120–125, <https://doi.org/10.1063/1.1731549>.
- [9] D.B. Miracle, *Acta Mater.* 61 (9) (2013) 3157–3171, <https://doi.org/10.1016/j.actamat.2013.02.005>.
- [10] T. Egami, Y. Waseda, *J. Non-Cryst. Solids* 64 (1984) 113–134, [https://doi.org/10.1016/0022-3093\(84\)9021-0-2](https://doi.org/10.1016/0022-3093(84)9021-0-2).
- [11] H.W. Sheng et al., *Nature* 439 (2006) 419–425, <https://doi.org/10.1038/nature04421>.
- [12] D.B. Miracle, *Nat. Mater.* 3 (2004) 697–702, <https://doi.org/10.1038/nmat1219>.
- [13] Y.Q. Cheng, E. Ma, H.W. Sheng, *Phys. Rev. Lett.* 102 (2009), <https://doi.org/10.1103/PhysRevLett.102.245501>.
- [14] K. Ahn et al., *Phys. Rev. B* 70 (2004), <https://doi.org/10.1103/PhysRevB.70.224103> 224103.
- [15] F. Yang et al., *Europhys. Lett.* 107 (2014) 46001, <https://doi.org/10.1209/0295-5075/107/46001>.
- [16] G.F. Weir et al., *Philos. Mag. B* 47 (1983) 163–176, <https://doi.org/10.1080/13642812.1983.9728428>.
- [17] D. Mayou et al., *Phys. Rev. B* 33 (1986) 3384–3391, <https://doi.org/10.1103/PhysRevB.33.3384>.
- [18] V. Schnabel et al., *J. Phys. Condes. Matter* 29 (2017), <https://doi.org/10.1088/1361-648X/aa72cb>.
- [19] Q. He et al., *Acta Mater.* 59 (2011) 202–215, <https://doi.org/10.1016/j.actamat.2010.09.025>.
- [20] C.C. Yuan et al., *Phys. Rev. Lett.* 107 (2011), <https://doi.org/10.1103/PhysRevLett.107.236403> 236403.
- [21] C.C. Yuan et al., *Appl. Phys. Lett.* 101 (2012), <https://doi.org/10.1063/1.4734390> 021902.
- [22] S.R. Nagel, J. Tauc, *Phys. Rev. Lett.* 35 (6) (1975) 380–383, <https://doi.org/10.1103/PhysRevLett.35.380>.
- [23] C.H. Shek, Y.M. Wang, C. Dong, *Mater. Sci. Eng. A* 291 (2000) 78–85, [https://doi.org/10.1016/S0921-5093\(00\)00979-5](https://doi.org/10.1016/S0921-5093(00)00979-5).
- [24] H.B. Yu, W.H. Wang, H.Y. Bai, *Appl. Phys. Lett.* 96 (2010), <https://doi.org/10.1063/1.3327337> 081902.
- [25] F.R. Wang, H.P. Zhang, M.Z. Li, *J. Alloy. Compd.* 763 (2018) 392–398, <https://doi.org/10.1016/j.jallcom.2018.05.344>.
- [26] U. Mizutani et al., *Phys. Rev. Lett.* 41 (1978) 661–664, <https://doi.org/10.1103/PhysRevLett.41.661>.
- [27] S. Hosokawa et al., *Acta Mater.* 55 (2007) 3413–3419, <https://doi.org/10.1016/j.actamat.2007.01.041>.
- [28] E. Babić et al., *Philos. Magazine* 98 (2018) 693–709, <https://doi.org/10.1080/14786435.2017.1415467>.
- [29] C. Fan et al., *Appl. Phys. Lett.* 89 (2006), <https://doi.org/10.1063/1.2345276> 111905.
- [30] P.H. Gaskell, *Nature* 276 (1978) 484–485, <https://doi.org/10.1038/276484a0>.
- [31] H. Eckert, *Prog. Nucl. Magn. Reson. Spectrosc.* 24 (1992) 159–293, [https://doi.org/10.1016/0079-6565\(92\)80001-V](https://doi.org/10.1016/0079-6565(92)80001-V).
- [32] J. Durand, P. Panissod, *J. Magn. Magn. Mater.* 31 (1983) 1567–1570, [https://doi.org/10.1016/0304-8853\(83\)91018-1](https://doi.org/10.1016/0304-8853(83)91018-1).
- [33] W.A. Hines et al., *J. Non-Cryst. Solids* 61 (1984) 1255–1260, [https://doi.org/10.1016/0022-3093\(84\)90714-2](https://doi.org/10.1016/0022-3093(84)90714-2).
- [34] C.S. Lue et al., *Phys. Rev. B* 71 (19) (2005), <https://doi.org/10.1103/PhysRevB.71.195104> 195104.
- [35] X.K. Xi et al., *J. Phys. Condes. Matter* 23 (2011), <https://doi.org/10.1088/0953-8984/23/1/115501>.
- [36] A.R. Ferreira, J.P. Rino, *Sci. Rep.* 7 (2017) 9305, <https://doi.org/10.1038/s41598-017-08919-6>.
- [37] Y. Zhang, N. Mattern, J. Eckert, *J. Alloy. Compd.* 514 (2012) 141–149, <https://doi.org/10.1016/j.jallcom.2011.11.034>.
- [38] C.C. Yuan, F. Yang, F. Kargl, D. Holland-Moritz, G.G. Simeoni, A. Meyer, *Phys. Rev. B* 91 (2015) 214203, <https://doi.org/10.1103/PhysRevB.91.214203>.
- [39] P. Yu, H.Y. Bai, M.B. Tang, W.L. Wang, *J. Non-Cryst. Solids* 351 (2005) 1328–1332, <https://doi.org/10.1016/j.jnoncrysol.2005.03.012>.
- [40] G. Kumar, T. Ohkubo, T. Mukai, K. Hono, *Scr. Mater.* 57 (2007) 173–176, <https://doi.org/10.1016/j.scriptamat.2007.02.013>.
- [41] P. Yu, H.Y. Bai, *Mater. Sci. Eng. A* 485 (2008) 1–4, <https://doi.org/10.1016/j.msea.2007.07.062>.
- [42] P.F. Paradis et al., *Mater. Sci. Eng. R* 76 (2014) 1–53, <https://doi.org/10.1016/j.mser.2013.12.001>.
- [43] T. Wada et al., *J. Mater. Res.* 24 (2009) 2941–2948, <https://doi.org/10.1557/JMR.2009.0348>.
- [44] K.M. Yu et al., *J. Non-Cryst. Solids* 488 (2018) 52–62, <https://doi.org/10.1016/j.jnoncrysol.2018.02.030>.
- [45] J.J.Z. Li et al., *Acta Mater.* 59 (2011) 2166–2171, <https://doi.org/10.1016/j.actamat.2010.12.017>.
- [46] L. Pauling, *J. Am. Chem. Soc.* 69 (1947) 542–553, <https://doi.org/10.1021/ja01195a024>.
- [47] E.A. Brandes, G.B. Brook (Eds.), *Smithells Metals Reference Book, Chapter 4: X-ray Analysis of Metallic Materials*, Butterworths, London, 1983, pp. 41–42.
- [48] R.F.W. Bader, *J. Phys. Chem. A* 102 (1998) 7314–7323, <https://doi.org/10.1021/jp981794v>.
- [49] A.L. Allred, *J. Inorg. Nucl. Chem.* 17 (1961) 215–221, [https://doi.org/10.1016/0022-1902\(61\)80142-5](https://doi.org/10.1016/0022-1902(61)80142-5).
- [50] J.D. Stevenson, J. Schmalian, P.G. Wolyne, *Nat. Phys.* 2 (2006) 268–274, <https://doi.org/10.1038/nphys261>.
- [51] Y. Gebremichael, M. Vogel, S.C. Glotzer, *J. Chem. Phys.* 120 (2004) 4415–4427, <https://doi.org/10.1063/1.1644539>.
- [52] P.F. Guan et al., *Phys. Rev. Lett.* 108 (2012), <https://doi.org/10.1103/PhysRevLett.108.175501> 175501.
- [53] T. Schenk et al., *Phys. Rev. Lett.* 89 (2002), <https://doi.org/10.1103/PhysRevLett.89.075507> 075507.
- [54] A. Inoue, *Acta Mater.* 48 (2000) 279–306, [https://doi.org/10.1016/S1359-6454\(99\)00300-6](https://doi.org/10.1016/S1359-6454(99)00300-6).
- [55] Q. Wang et al., *Sci. Rep.* 4 (2014) 4648, <https://doi.org/10.1038/srep04648>.
- [56] P. Ganesh, M. Widom, *Phys. Rev. B* 77 (1) (2008), <https://doi.org/10.1103/PhysRevB.77.014205> 014205.
- [57] H. Wang, T. Hu, T. Zhang, *Physica B* 411 (2013) 161–165, <https://doi.org/10.1016/j.physb.2012.11.044>.
- [58] A.J. Drehman, A.L. Greer, D. Turnbull, *Appl. Phys. Lett.* 41 (1982) 716–717, <https://doi.org/10.1063/1.93645>.
- [59] Q. Wang et al., *Phys. Rev. B* 83 (2011), <https://doi.org/10.1103/PhysRevB.83.014202> 014202.
- [60] C. Chattopadhyay et al., *Mater. Sci. Tech.* 32 (2016) 380–400, <https://doi.org/10.1179/1743284715Y.0000000104>.
- [61] S. Guo, Z.P. Lu, C.T. Liu, *Intermetallics* 18 (2010) 883–888, <https://doi.org/10.1016/j.intermet.2009.12.025>.
- [62] A.F. Kozmidis-Petrovic, *Thermochim. Acta* 523 (2011) 116–123, <https://doi.org/10.1016/j.tca.2011.05.011>.
- [63] D. Turnbull, *Contemp. Phys.* 10 (1969) 473–488, <https://doi.org/10.1080/00107516908204405>.
- [64] Z.P. Lu, C.T. Liu, *Acta Mater.* 50 (13) (2002) 3501–3512, [https://doi.org/10.1016/S1359-6454\(02\)00166-0](https://doi.org/10.1016/S1359-6454(02)00166-0).
- [65] A.N. Trukhin, *J. Non-Cryst. Solids* 189 (1995) 1–15, [https://doi.org/10.1016/0022-3093\(95\)00207-3](https://doi.org/10.1016/0022-3093(95)00207-3).
- [66] P.N. Pusey, W. van Meegen, *Phys. Rev. Lett.* 59 (1987) 2083–2086, <https://doi.org/10.1103/PhysRevLett.59.2083>.
- [67] K.A. Gschneidner et al., *Acta Mater.* 57 (2009) 5876–5881, <https://doi.org/10.1016/j.actamat.2009.08.012>.
- [68] M.E. Eberhart, *Acta Mater.* 44 (1996) 2495–2504, [https://doi.org/10.1016/1359-6454\(95\)00347-9](https://doi.org/10.1016/1359-6454(95)00347-9).
- [69] C.E. Lekka, G.A. Evangelakis, *Scr. Mater.* 61 (10) (2009) 974–977, <https://doi.org/10.1016/j.scriptamat.2009.08.008>.
- [70] C.C. Yuan, Y.F. Yang, X.K. Xi, *J. Appl. Phys.* 114 (21) (2013), <https://doi.org/10.1063/1.4837999> 213511.
- [71] K.B. Kim et al., *Appl. Phys. Lett.* 89 (2006), <https://doi.org/10.1063/1.2337534>.
- [72] W. Liu et al., *Nat. Commun.* 7 (2016) 13497, <https://doi.org/10.1038/ncomms13497>.
- [73] G. Kresse, J. Furthmüller, *Comp. Mater. Sci.* 6 (1996) 15–50, [https://doi.org/10.1016/0927-0256\(96\)00008-0](https://doi.org/10.1016/0927-0256(96)00008-0).